# Thiolato-Activated Oxo−Metal Bond Features in Molybdenum and Tungsten Oxidoreductase Models As Revealed by Raman Spectroscopy

**Hiroyuki Oku, Norikazu Ueyama, and Akira Nakamura***,†

Department of Macromolecular Science, Faculty of Science, Osaka University, Toyonaka, Osaka 560, Japan, and the Institute for Molecular Science, Okazaki, Aichi 444, Japan

*Received September 30, 1994*[⊗]

Resonance Raman spectra have been obtained for $(PPh_4)_2[Mo^{VI}O_2(1,2\text{-dicyanoethylene-}1,2\text{-dithiolato})_2]\cdot 2MeOH$ (**1**), $(NEt_4)_2[M^{VI}O_2(1,2\text{-benzenedithiolato})_2]$ (M = W (**3a**) and Mo (**4a**)), $(NEt_4)_2[Mo^{VI}O_2(3,4\text{-toluenedithiolato})_2]$ (**5**), *in situ* formed $(NEt_4)_2[Mo^{VI}O_2(1,2\text{-bis(methoxycarbonyl)ethylene-}1,2\text{-dithiolato})_2]$ (**2**), $(PPh_4)_2[Mo^{IV}O(1,2\text{-dicyanoethylene-}1,2\text{-dithiolato})_2]$ (**6**), and $(NEt_4)_2[M^{IV}O(1,2\text{-benzenedithiolato})_2]$ (M = W (**8**) and Mo (**9**)) which are related to the active site of molybdenum and tungsten oxidoreductases. For **1**, **3a**, **4a**, and **5**, $\nu_s$ and $\nu_{as}$ $M^{VI}$=O bands are observed in the 885 − 858 and 851 − 835 $cm^{-1}$ ranges, respectively, which appear at a quite low wavenumber region, due to the $M^{VI}$=O bond activation by the mutual *trans* influence with the thiolato. The excitation profiles of the $\nu_s(M^{VI}=O)$ band for **1**, **3a**, **4a**, and **5** show clear enhancement at 700 − 600 nm in the lowest-energy region of LMCT bands. The cause of the enhancement is attributable to the vibronic coupling of similar geometric changes between the symmetric $M^{VI}$=O stretching and the substantial elongation of the $M^{VI}$=O bond when an excited electron half occupies the LUMO ($M^{VI}$=O antibonding). For the dithiolene complexes, **1**, **2**, **6**, and **7**, the $\nu$(C=C) bands (range 1472 − 1535 $cm^{-1}$) are observed at a lower region than those of dimethyl sulfoxide reductase (1568 (oxidized state) and 1575 $cm^{-1}$ (reduced state)). Although the frequency shift upon oxidation of dimethyl sulfoxide reductase is +7 $cm^{-1}$, those of the model complexes are −19 (for **1** and **6**) and −32 $cm^{-1}$ (for **2** and **7**). These dithiolene frequencies of the enzyme are very anomalous compared with the various dithiolene compounds.

## Introduction

Molybdenum[1] and tungsten oxidoreductases,[2] e.g., sulfite oxidase,[1] dimethyl sulfoxide (DMSO) reductase,[3] xanthine oxidase,[1] formate dehydrogenase,[1,4] and aldehyde oxidoreductase[5,6] are thought to participate in the metabolism of small molecules and the respiratory chain by use of the O-atom transfer reaction.[7] In the active site, the pterin-substituted molybdenum (or tungsten) ene-1,2-dithiolate structure has been assumed for these molybdenum[8] and tungsten[9,10] enzymes. The EXAFS spectroscopic analyses of the oxidized-state enzymes sulfite oxidase[11] and aldehyde-ferredoxin oxidoreductase[12] have shown the presence of *cis*-$(Mo^{VI}O_2)^{2+}$ and *cis*-$(W^{VI}O_2)^{2+}$ centers, respectively, surrounded by at least three sulfur ligands in the active site. The chelation by the dithiolene group of the pterin cofactor in molybdenum or tungsten oxidoreductase should place one of the thiolate ligands *trans* to $Mo^{VI}$(or $W^{VI}$)=O, if the $(Mo^{VI}O_2)^{2+}$ or $(W^{VI}O_2)^{2+}$ center is assumed to have an octahedral structure. In the case of DMSO reductase, the resonance Raman[13] (oxidized and reduced states which are considered to be Mo(VI) and Mo(IV) state, respectively) and variable-temperature MCD[14] (Mo(V) state) studies have implicated the chelating coordination of dithiolene to the molybdenum center.

However, only three examples of the structurally characterized $(Mo^{VI}O_2)^{2+}$ or $(W^{VI}O_2)^{2+}$ complex having the one thiolate ligand *trans* to the $Mo^{VI}$(or $W^{VI}$)=O group have been reported, e.g. bis(1,2-benzenedithiolato)dioxomolybdenum(VI)[15,16] or -tung-

[⊗] Abstract published in *Advance ACS Abstracts,* June 15, 1995.

(1) (a) Wootton, J. C.; Nicolson, R. E.; Cock, J. M.; Walters, D. E.; Burke, J. F.; Doyle, W. E.; Bray, R. C. *Biochem. Biophys. Acta.* **1991**, *1057*, 157. (b) Bray, R. C. *Q. Rev. Biophys.* **1988**, *21*, 299−329. (c) *Molybdenum Enzymes, Cofactors, and Model Systems*; Stiefel, E. I.; Coucouvanis, D. C.; Newton, W. E. Eds.; American Chemical Society: Washington, DC, 1993. (d) *Metalloproteins*; Otsuka, S.; Yamanaka, T. Eds.; Kodansha Ltd.: Tokyo, Elsevier: Amsterdam, 1988. (e) *Molybdenum Enzymes*; Spiro, T. G., Ed.; John Wiley & Sons: New York, 1985. (f) *Molybdenum Chemistry of Biological Signifcance*; Newton, W. E. ; Otsuka, S. Eds.; Plenum Press: New York, 1980. (g) Young, C. G.; Wedd, A. G. In *Encyclopedia of Inorganic Chemistry*; R. B. King, Ed.; John Wiley and Sons: Chichester, 1994; Vol. 5, p 2320.

(2) (a) Adams, M. M. W. In *Encyclopedia of Inorganic Chemistry*; King, R. B., Ed.; John Wiley and Sons: Chichester, 1994; Vol. 8, p 4284. (b) Adams, M. W. W. *Annu. Rev. Microbiol.* **1993**, *47*, 627.

(3) Yamamoto, Y.; Saiki, T.; Liu, S.-M.; Ljungdahl, L. G. *J. Biol. Chem.* **1983**, *258*, 1826.

(4) White, H.; Strobl, G.; Feicht, R.; Simon, H. *Eur. J. Biochem.* **1989**, *184*, 89.

(5) White, H.; Feicht, R.; Huber, C.; Lottspeich, F.; Simon, H. *Biol. Chem. Hoppe-Seyler* **1991**, *372*, 999.

(6) (a) Mukund, S.; Adams, M. W. W. *J. Biol. Chem.* **1990**, *265*, 11508. (b) Mukund, S.; Adams, M. W. W. *J. Biol. Chem.* **1991**, *266*, 14208.

(7) (a) Holm, R. H. *Coord. Chem. Rev.* **1990**, *100*, 183. Holm, R. H. *Chem. Rev.* **1987**, *87*, 1401. Holm, R. H.; Berg, J. M. *Acc. Chem. Res.* **1986**, *19*, 363−370. (b) Murray, K. N.; Watson, J. G.; Chaykin, S. *J. Biol. Chem.* **1966**, *244*, 4798. (c) Hille, R.; Sprecher, H. *J. Biol. Chem.* **1987**, *262*, 10914.

(8) (a) Cramer, S. P.; Johnson, J. L.; Ribeiro, A. A.; Millington, D. S.; Rajagopalan, K. V. *J. Biol. Chem.* **1987**, *262*, 16357. (b) Johnson, J. L.; Bastian, J. L.; Rajagopalan, K. V. *Proc. Natl. Acad. Sci. U.S.A.* **1990**, *87*, 3190. (c) Borner, G.; Karrasch, M.; Thauer, R. K. *FEBS Lett.* **1991**, *290*, 31.

(9) Schwitz, R. A.; Richter, M.; Linder, D.; Thauer, R. K. *Eur. J. Biochem.* **1992**, *207*, 559.

(10) (a) Johnson, J. L.; Rajagopalan, K. V.; Munkund, S.; Adams, M. W. W. *J. Biol. Chem.* **1993**, *268*, 4848. (b) Schmitz, R. A.; Richter, M.; Linder, D.; Thauer, R. K. *Eur. J. Biochem.* **1992**, *207*, 559.

(11) George, G. N.; Kipke, C. A.; Prince, R. C.; Sunde, R. A.; Enemark, J. H.; Cramer, S. P. *Biochemistry* **1989**, *28*, 5075.

(12) George, G. N.; Prince, R. C.; Mukund, S.; Adams, M. W. W *J. Am. Chem. Soc.* **1992**, *114*, 3521.

(13) Gruber, S.; Kilpatrick, L.; Bastian, N. R.; Rajagopalan, K. V.; Spiro, T. G. *J. Am. Chem. Soc.* **1990**, *112*, 8180.

(14) (a) Benson, N.; Farrar, J. A.; McEwan, A. G.; Thomson, A. J. *FEBES Lett.* **1992**, *307*, 169. (b) Finnegan, M. G.; Hilton, J.; Rajagopalan, K. V.; Johnson, M. K. *Inorg. Chem.* **1993**, *32*, 2616.

(15) Yoshinaga, N.; Ueyama, N.; Okamura, T.; Nakamura, A. *Chem. Lett.* **1990**, 1655.

0020-1669/95/1334-3667$09.00/0 

sten(VI)[17] and bis(1,2-dicyanoethylene-1,2-dithiolato)dioxomolybdenum(VI) complexes.[16,18] This type of complex has been thought to be unstable due to the mutual *trans* influence of a $Mo^{VI}$=O group and one of the *trans* positioned thiolate ligands.[19]

Vibrational spectroscopy has been used extensively to reveal the bonding nature of some molybdenum thiolates and some dithiolene complexes.[20-28] Resonance Raman spectroscopy in particular provides electronic features. Thus, enhanced Raman lines have been reported for $\nu$(C=C), $\nu$(Mo=O), and $\nu$(Mo−S) bands of various molybdenum complexes which are excited by charge-transfer (CT) transitions.[21-26] Previously, we reported the highly enhanced Raman line assigned to the Mo=O vibration for oxomolybdenum(V) bis-($\mu$-oxo) and bis($\mu$-sulfido) complexes as a model study of molybdenum-containing enzymes.[21] Subramanian et al. have reported[22] the resonance Raman characteristics for three model complexes, $[Mo^{VI}O_2(dttd)]$ (**10**),[29] $(NEt_4)_2[Mo^{IV}O(S_2C_2(COOMe)_2)_2]$ (**7**),[29] and $(NEt_4)_2[Mo^{IV}(S_2C_2(COOMe)_2)_3]$, in order to estimate the optimum excitation wavelengths for protein studies. The resonance Raman properties of the $\nu(Mo^{V}=S)$ band for the complex $LMo^{V}OCl_2$ (L = hydrotris(3,5-dimethyl-1-pyrazolyl)borate) have been compared with that of the $\nu(Mo^{V}=O)$ band for the oxo analog by Backes et al.[26] because the terminal sulfide has been regarded as the active-site ligand of xanthine oxidase. Clark et al.[23] have discussed the resonance Raman enhancement in relation to the electronic spectra and the electronic configurations for some of the molybdenum(IV) and tungsten(IV) dithiolene complexes.

For molybdenum enzymes, the active site structure has also been investigated by resonance Raman spectroscopy. Relevant reports are found for the molybdenum domain of rat liver sulfite oxidase,[27] DMSO reductase,[13] and milk xanthine oxidase.[28] Particularly, a detailed study was carried out for DMSO reductase. The redox (reduced and oxidized state) associated shift of the band at the C=C stretching region and $^{34}S$ shifts of Mo−S bands in the 300 − 400 $cm^{-1}$ range were taken to suggest dithiolene coordination to the molybdenum center.[13] In the model study, $^{34}S$ enrichment was reported only by Pilato et al.[32] They reported a $^{34}S$-shifted band at 350 $cm^{-1}$ with the use of a pterin-substituted ene-1,2−dithiolate complex, $[Cp_2Mo^{IV}(S_2C_2(C(O)CH_3)(N\text{-pivaloyl-6-pterin}))]$. Therefore, this dithiolene model study also supported the $^{34}S$-shifted band in the reduced-state DMSO reductase as $Mo^{IV}$−S stretchings.

In this situation, in order to elucidate the nature of the activated oxo−metal bond, it is important to examine the resonance Raman patterns of the model compounds enhanced by the influence of *trans* thiolate coordination. The partial charge transfer by the thiolate is thus considered to contribute to the observed high oxidation reactivity of the enzyme active site.

In this paper, we describe resonance Raman characteristics for Mo(VI) and W(VI) complexes as models of the oxidized state of molybdenum and tungsten oxidoreductases. These complexes have two oxo- and two dithiolene-type ligands in octahedral coordination and are useful in clarifying the nature of activated oxo ligand and to comparing their spectra with the Raman bands observed in molybdenum enzymes.

## Experimental Section

All operations were carried out under an argon atmosphere. *N,N*-Dimethylformamide (DMF) and dimethyl sulfoxide (DMSO) were purified by distillation before use.

**Materials.** Preparation of $(PPh_4)_2[Mo^{VI}O_2(S_2C_2(CN)_2)_2]\cdot 2MeOH$ (**1**),[29] $(NEt_4)_2[W^{VI}O_2(S_2C_6H_4)_2]$ (**3a**),[29] $(PPh_4)_2[W^{VI}O_2(S_2C_6H_4)_2]$ (**3b**), $(NEt_4)_2[Mo^{VI}O_2(S_2C_6H_4)_2]$ (**4a**), $(PPh_4)_2[Mo^{VI}O_2(S_2C_6H_4)_2]$ (**4b**), $(NEt_4)_2[Mo^{VI}O_2(S_2C_6H_3Me)_2]$ (**5**),[29] $(PPh_4)_2[Mo^{IV}O(S_2C_2(CN)_2)_2]$ (**6**), $(NEt_4)_2[Mo^{IV}O(S_2C_6H_4)_2]$ (**9**), and $(NEt_4)_2[W^{IV}O(S_2C_6H_4)_2]$ (**8**) were previously reported[16,18,33-35] $(NEt_4)_2[Mo^{IV}O(S_2C_2(COOMe)_2)_2]$ (**7**) was synthesized by the reported procedure.[36]

**Physical Measurements.** The absorption spectra were recorded on a Jasco Ubest-30 spectrophotometer with use of a 1 mm cell under an argon atmosphere. The extinction coefficients were given in $M^{-1}$ $cm^{-1}$. Raman spectra were taken on Jasco R-800, NR-1800, and RFT-200 spectrophotometers equipped with an HTV-R649 photomultiplier, a liquid $N_2$ cooled CCD detector, and a liquid $N_2$ cooled InGaAs detector, respectively, at 298 K. Exciting radiation was provided by $Ar^+$ ion (457.9, 476.5, 488.0, 496.5, 501.7, and 514.5 nm), He−Ne (632.8 nm), $Kr^+$ ion (647.1 and 676.4 nm) or Nd:YAG laser (1064 nm). Wavenumbers of the Raman bands $\nu$(C=C), $\nu$(M=O), and $\nu$(M−S) (M = Mo and W) are determined from the expanded spectra at each region (conditions: 100−50 mW laser power (not focused on the sample), 5 $cm^{-1}$ slit width, 1−5 s dwell time/1.0 $cm^{-1}$ step, 8−64 scans), and calibrations were carried out with natural emissions of a neon lamp from 0 to 2000 $cm^{-1}$ as standard.

**Kinetic Measurements.** Reaction systems containing the monooxomolybdenum(IV) complex **6** or **7** and 10 equivs of $Me_3NO$ were monitored spectrophotometrically in the region 260−800 nm. A typical measurement was carried out in a 1 mm UV cell containing a solution of monooxomolybdenum(IV) dithiolato complex (ca. 1 mM in DMF)

(16) Ueyama, N; Oku, H.; Kondo, M; Okamura, T.; Yoshinaga, N.; Nakamura, A. Submitted to *Inorg. Chem.*
(17) Ueyama, N; Oku, H.; Nakamura, A. *J. Am. Chem. Soc.* **1992**, *114*, 7310.
(18) Oku, H.; Ueyama, N.; Nakamura, A.; Kai, Y.; Kanehisa, N. *Chem. Lett.* **1994**, 607.
(19) (a) Berg, J. M.; Hodgson, K. O.; Cramer, S. P.; Corbin, J. L.; Elseberry, A.; Pariyadath, N.; Stiefel, E. I. *J. Am. Chem. Soc.* **1979**, *101*, 2774. (b) Miller, K. F.; Bruce, A. E.; Pariyadath, N.; Heinecke, J.; Corbin, J. L.; Berg, J. M.; Hodgson, K. O. In *Molybdenum Chemistry of Biological Significance*; Plenum Press: New York, 1980; p 279.
(20) (a) McCleverty, J. A. *Prog. Inorg. Chem.* **1968**, *10*, 49. Burns, R. P.; McAuliffe, C. A. *Adv. Inorg. Chem. Radiochem.* **1979**, *22*, 303. (b) Fresco, J.; Sümann, O. *Inorg. Chem.* **1971**, *10*, 297. (c) Willis, L. J.; Loehr, T. M. *Spectrochim. Acta* **1987**, *43A*, 51. (d) Willis, L. J.; Loehr, T. M.; Miller, K. F.; Bruce, A. E.; Stiefel, E. I. *Inorg. Chem.* **1986**, *25*, 4289.
(21) (a) Ueyama, N.; Nakata, M.; Nakamura, A.; Yamashita, S.; Yamashita, T. *Inorg. Chem.* **1981**, *20*, 1934−1937. (b) Ueyama, N.; Nakata, M.; Nakamura, A.; Yamashita, S.; Yamashita, T. *Chem. Lett.* **1979**, 421.
(22) Subramanian, P.; Burgayer, S.; Richards, S.; Szalaki, V.; Spiro, T. G. *Inorg. Chem.* **1990**, *29*, 3849.
(23) Clark, R. J. H.; Turtle, P. C. J. *J. Chem. Soc., Dalton Trans.* **1978**, 1714.
(24) Müller, A.; Dieman, E. J. *J. Chem. Phys.* **1974**, *61*, 5469.
(25) Lincoln, S. E.; Loehr, T. M. *Inorg. Chem.* **1990**, *29*, 1990.
(26) Backes, G.; Enemark, J. H.; Loehr, T. M. *Inorg. Chem.* **1991**, *30*, 1839.
(27) (a) Griffith, W. P. *J. Chem. Soc. A* **1969**, 211. (b) Griffith, W. P.; Wickins, T. D. *J. Chem. Soc. A* **1968**, 1968.
(28) Schlapfer, C. W.; Nakamoto, K. *Inorg. Chem.* **1975**, *14*, 1338.
(29) Abbreviations used: $S_2C_2(COOMe)_2$ = 1,2-bis(methoxycarbonyl)-ethylene-1,2-dithiolate; dttd = 2,3:8,9-dibenzo-1,4,7,10-tetrathiadecane; $S_2C_6H_4$ = 1,2-benzenedithiolate; $S_2C_6H_3Me$ = 3,4-toluenedithiolate; $S_2C_2(CN)_2$ = 1,2-dicyanoethylene-1,2-dithiolate.
(30) Cited as unpublished results by: Garner, C. D.; Bristow, S. In *Molybdenum Enzymes*; Spiro, T. G., Ed.; Wiley: New York, 1985; pp 376.
(31) Oertling, W. A.; Hille, R. *J. Biol. Chem.* **1990**, *265*, 17446.
(32) (a) Pilato, R. S.; Eriksen, K.; Greaney, M. A.; Stiefel, E. I.; Goswami, S.; Kilpatrick, L.; Spiro, T. G.; Taylor, E. C.; Rheingold, A. L. *J. Am. Chem. Soc.* **1991**, *113*, 9372. (b) Pilato, R. S.; Eriksen, K.; Greaney, M. A.; Gea, Y.; Taylor, E. C.; Goswami, S.; Kilpatrick, L.; Spiro, T. G.; Rheingold, A. L.; Stiefel, E. I. In ref 1b, Chapter 6, p 83.
(33) A different procedure for the synthesis of $(PPh_4)_2[Mo^{IV}O(S_2C_2(CN)_2)_2]$ (**5**) has been reported by McCleverty, J. A.; Locke, J.; Ratcliff, B.; Wharton, E. *Inorg. Chim. Acta* **1969**, *3*, 283.
(34) The related complexes $(Q)_2[Mo^{VI}O_2(S_2C_2(CN)_2)_2]$ (Q = $PBu_4$ and $NBu_4$) have been reported. (a) Sarkar, S.; Das, S. K. *Proc. Indian Acad. Sci., Chem. Sci.* **1992**, 104, 437. (b) Das, S. K.; Chaudhury, P. K.; Biswas, D.; Sarkar, S. *J. Am. Chem. Soc.* **1994**, *116*, 9061.
(35) Oku, H.; Ueyama, N.; Nakamura, A. *Inorg. Chem.* **1994**, *33*, 209.
(36) Coucouvanis, D.; Hadjikyriacou, A.; Toupadakis, A.; Koo, S.; Ileperuma, O.; Draganjac, M.; Salifoglou, A. *Inorg. Chem.* **1991**, *30*, 754.

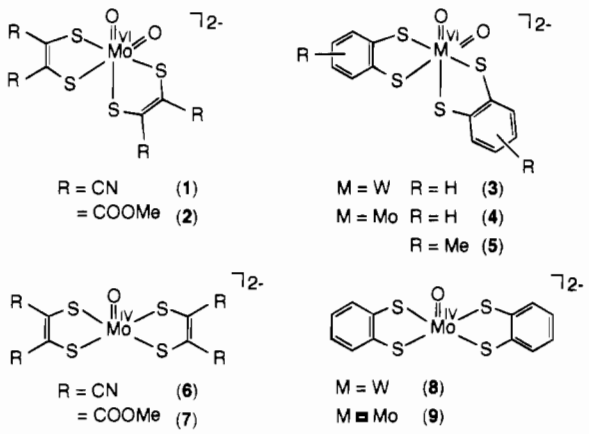


**Figure 1.** Structural diagrams of $(M^{VI}O_2)^{2+}$ and $(M^{IV}O)^{2+}$ (M = Mo and W) dithiolate complexes.

**Table 1.** Wavenumbers ($cm^{-1}$) of the Raman bands of $(M^{VI}O_2)^{2+}$ (M = Mo and W) Thiolate Complexes, **1**, **3a**, **4a**, and **5**

| complex | $\nu_s(M{=}O)$ $\nu_{as}(M{=}O)$ | $\nu(M{-}S)$ | $\nu(C{=}C)$ |
|---|---|---|---|
| $(PPh_4)_2[Mo^{VI}O_2(S_2C_2(CN)_2)_2]\cdot$ 2MeOH (**1**) | 885 | 354 | 1472 |
| | 851 | 330 | |
| | | 313 | |
| $(NEt_4)_2[W^{VI}O_2(S_2C_6H_4)_2]$ (**3a**) | 885 | 370 | |
| | 843 | 352 | |
| | | 326 | |
| $(NEt_4)_2[Mo^{VI}O_2(S_2C_6H_4)_2]$ (**4a**) | 858 | 356 | |
| | 829 | 322 | |
| $(NEt_4)_2[Mo^{VI}O_2(S_2C_6H_3Me)_2]$ (**5**) | 863 | 381 | |
| | 835 | 358 | |
| | | 329 | |
| | | 318 | |

at 27 °C. After thermal equilibrium, a $Me_3NO$ solution (ca.100 mM in DMF, also at 27 °C) was injected through a silicone rubber cap, and the cell contents were quickly mixed by shaking. The time dependence of the absorbance of the dioxomolybdenum(VI) complex was measured every 1.0 h. The calculations for the data analysis were performed at 420 nm.

**Detection of $(NEt_4)_2[Mo^{VI}O_2(S_2C_2(COOMe)_2)_2]$ (2).** A reaction system containing the $(Mo^{IV}O)^{2+}$ complex **7** (4 mM) and 10 equiv of $Me_3NO$ in DMSO or DMSO-$d_6$ was monitored spectrophotometrically in the 350 to 800 nm region for 11.5 h at 27 °C. After the detection of anabsorbance at 530 nm, the Raman spectra were measured within 90 min, with 632.8 nm line excitation, on a Jasco R-800 spectrophotometer. At $^1$H-NMR spectrum was also recorded on a JEOL-EX-270 spectrometer. The signal from the solvent at 2.50 ppm was used as standard.

**Molecular Orbital Calculations.** *Ab initio* calculations with the restricted Hartree–Fock procedure for $[Mo^{VI}O_2(S_2C_6H_4)_2]^{2-}$ and $[Mo^{VI}O_2$-(dttd)] structure were performed on a SPARTAN software package (Wavefunction Inc., 1993). The STO-3G basis set was chosen. The atomic coordinates were taken from each crystal structure for the anion part of $(PPh_4)_2[Mo^{VI}O_2(S_2C_6H_4)_2]$ (**4b**)[16] and $[Mo^{VI}O_2(dttd)]$ (**10**).[37]

## Results

**Raman Spectra of $(M^{VI}O_2)^{2+}$ (M = Mo and W) Dithiolato Complexes 1, 3a, 4a, and 5.** Structural diagrams of the $(M^{VI}O_2)^{2+}$ (M = Mo and W) thiolato complexes are shown in Figure 1. Figures 2 and 3a–c show the Raman spectra of **1**, **3a**, **4a**, and **5**, respectively, in the solid state with 632.8 or 514.5 nm excitation. Table 1 lists the Raman bands of **1**, **3a**, **4a**, and **5**. The assignable band frequencies of $M^{VI}{=}O$ and $M^{VI}{-}S$ stretchings are near the range reported by Willis et al.[20d] and Subramanian et al.[22]

In the spectra, two intense bands were observed in the regions 885–858 and 851–835 $cm^{-1}$ assignable to $\nu_s$ and $\nu_{as}$[32] $M^{VI}{=}O$ stretchings, respectively. The two $M^{VI}{=}O$ bands appear in a quite low wavenumber region compared with the Raman bands for a thioether complex, $[Mo^{VI}O_2(dttd)]$ (**10**), at 922 and 890 $cm^{-1}$ [22] and for a dithiocarbamate complex, $[M^{VI}O_2(S_2CNMe_2)_2]$ at 938 and 898 $cm^{-1}$ (M = Mo) and 940 and 900 $cm^{-1}$ (M = W).[38]

The $\nu(M^{VI}{-}S)$ associated bands for **1**, **3a**, **4a** and **5** were expected to appear below 400 $cm^{-1}$.[21,22] According to the vibrational analysis based on a simplified *cis*-$MO_2S_4$ skeleton model ($C_{2v}$ symmetry)[39] where chelation effects are ignored and coupling between M–S and S–C stretches is assumed to be small,[40] normal modes for an ideal octahedron consist of two symmetric ($A_1$) and two asymmetric ($B_1$) M–S stretching modes and one symmetric ($A_1$) and one asymmetric ($B_1$) M=O stretching modes. The situation should be different in our dithiolato model complexes. Due to the long and short $M^{VI}{-}S$ bonds, the spectra of the $\nu(M^{VI}{-}S)$ region were complicated because there are short and long $M^{VI}{-}S$ bonds observed in the crystal structures of **1**, **3a**, **4a**, and **5**. The short $M^{VI}{-}S$ distances are 2.439(2) Å for **1**, 2.416(3) and 2.433(3) Å for **3b**, 2.425(4) and 2.424(4) Å for **4a**, and 2.421(3) and 2.440(2) Å for **4b**. The long, thioether-like $M^{VI}{-}S$ distances are 2.604(3) Å for **1**, 2.590(3) and 2.604(3) Å for **3b**, 2.543(4) and 2.601(4) Å for **4a**, and 2.596(3) and 2.612(3) Å for **4b**. To assign the metal–sulfur stretching band, we have compared the spectrum of W(VI) complex **3a** with that of an analogous Mo(VI) complex **4a** (i.e., metal substitution). For **3a** and **4a**, almost the same $M^{VI}{-}S$ bond nature was expected because tungsten an has an equal covalent radius to that of molybdenum. Actually, similar $M^{VI}$EnDash–S bond distances were observed for the W(VI) complex **3b** (mean, 2.597(10) and 2.425(12) Å) and the Mo(VI) complex **4b** (mean, 2.604(11) and 2.431(13) Å). As a result of comparison, the probable $M^{VI}{-}S$ bands are at 370, 352, and 326 $cm^{-1}$ for the W(VI) complex **3a** and at 356 and 322 $cm^{-1}$ for the Mo(VI) complex **4a**. For the other Mo(VI) complexes, **1** and **5**, which have $S_2C_2(CN)_2$ and $S_2C_6H_3Me$ ligands, respectively, numerous bands were observed in the range 400–300 $cm^{-1}$. Those bands at 354, 330, and 310 $cm^{-1}$ for **1** and 381, 358, 329, and 318 $cm^{-1}$ for **5** are presumably $Mo^{VI}{-}S$-related bands.

In the complicated regions (below 400 $cm^{-1}$) of the spectra of **1**, **2a**, **3b** and **4**, there should be two types of Mo–S stretches. One is from the long $M^{VI}{-}S$ (*trans* to oxo) bond (2.60 Å). The other is from the short $M^{VI}{-}S$ (*cis* to oxo) bond (2.43 Å). The vibrations of the long $M^{VI}{-}S$ bond are expected at lower frequencies, compared with that of the short $M^{VI}{-}S$ bond. A similar example has been reported by Subramanian et al.,[22] for $[Mo^{VI}O_2(dttd)]$ (**10**), which has long $Mo^{VI}{-}S$ (thiolate) and short $Mo^{VI}{-}S$ (thioether) bond distances (2.68 and 2.40 Å, respectively). They expected long $Mo^{VI}{-}S$ (thioether) frequencies at −250 $cm^{-1}$ on the basis of bond Badger's rule.[41] In our case, application of this rule to the long $Mo^{VI}{-}S$ (*trans* to oxo) bond suggests that the $Mo^{VI}{-}S$ frequency should be ~20% lower than that of the short $Mo^{VI}{-}S$ bond and therefore should occur at ~300 $cm^{-1}$. Unfortunately, there are no strong bands in the corresponding region.

(37) Yu, S.; Holm, R. H. *Inorg. Chem.* **1989**, *28*, 4385.

(38) Kaul, B. B.; Enemark, J. H.; Merbs, S. L.; Spence, J. T. *J. Am. Chem. Soc.* **1985**, *107*, 2885.

(39) Saito, H; Nakamoto, K. In *Kireto Kagaku (Chelate Chemistry)*; Keihei, U. Ed.; Nankodo: Tokyo, 1976; Vol. 1, Chapter 3.

(40) Tatsumi, K.; Matsubara, I.; Inoue, Y.; Nakamura, A.; Miki, K.; Kasai, N. *J. Am. Chem. Soc.* **1989**, *111*, 7766.

(41) (a) Hershbach, D. R.; Laurie, V. W. *J. Chem. Phys.* **1961**, *35*, 458. (b) Badger, R. M. *J. Chem. Phys.* **1935**, *3*, 710.

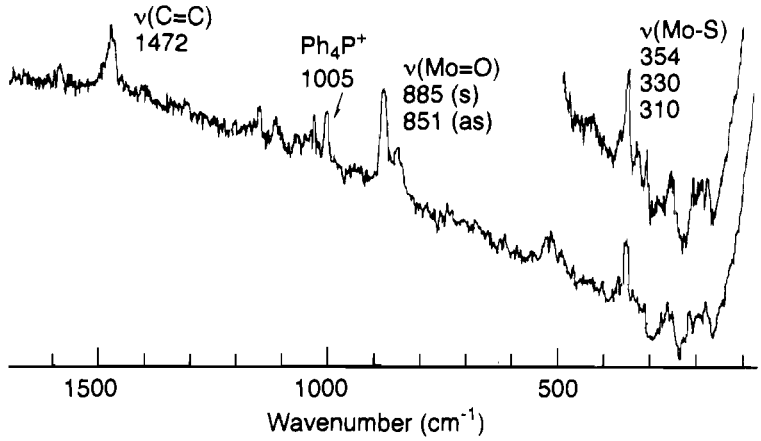


**Figure 2.** Raman spectra of $(PPh_4)_2[Mo^{VI}O_2(S_2C_2(CN)_2)_2]\cdot 2MeOH$ (**1**) (632.8 nm excitation, 50 mW laser power, 5 $cm^{-1}$ slit width, 5 s dwell time/5.0 $cm^{-1}$ step (1.0 $cm^{-1}$ step for vertical-scale-expanded spectrum), 42 scans) in the solid state, KBr disk.

**Raman Excitation Profiles for $(M^{VI}O_2)^{2+}$ (M = Mo and W) Complexes 1, 3a, 4a, and 5.** Figures 4 and 5a–c show the Raman excitation profiles of $\nu_s(M^{VI}{=}O)$, $\nu(M^{VI}{-}S)$, and $\nu(C{=}C)$ (only for **1**) bands (M = W or Mo) for **1**, **3a**, **4a**, and **5**. The enhancements of all resonance Raman vibrations were normalized to the peak intensity of the 1005 $cm^{-1}$ (for $PPh_4^+$) or 483 $cm^{-1}$ (for $NEt_4^+$) band of the countercation. The absorption spectra of **1**, **3a**, **4a**, and **5** are inset in each figure.

**$(PPh_4)_2[Mo^{VI}O_2(S_2C_2(CN)_2)_2]\cdot 2MeOH$ (1).** The absorption spectrum of this complex in the visible region shows $\lambda_{max}$ at 420 nm ($\epsilon$ = 7600 $M^{-1}$ $cm^{-1}$) and 522 nm ($\epsilon$ = 1600 $M^{-1}$ $cm^{-1}$). The band at 885 $cm^{-1}$ assignable to $\nu_s(Mo^{VI}{=}O)$ and the band at 1472 $cm^{-1}$ assignable to $\nu(C{=}C)$ are intensified by irradiation at longer (676.4 nm) and shorter (457.9 nm) wavelengths. The intensity enhancements are clearly shown by comparison with the band intensities at the off-resonance region of 1064 nm. In the case of a $\nu(Mo^{VI}{-}S)$ band at 354 $cm^{-1}$, a relatively weak enhancement was observed from 676.4 nm ($I/I_{1005\ cm^{-1}}$ = 0.66) to 457.9 nm ($I/I_{1005\ cm^{-1}}$ = 0.25). The enhancement maxima are found at 632.8–647.9 nm and 496.5 nm which are in the same region with those of the $\nu_s(Mo^{VI}{=}O)$- and $\nu(C{=}C)$ bands.

**$(NEt_4)_2[W^{VI}O_2(S_2C_6H_4)_2]$ (3a).** The absorption maxima were observed at 483 (1300) and 419 nm (2300 $M^{-1}cm^{-1}$). The 12–13 fold increase in intensity of the $\nu_s(W^{VI}{=}O)$ band at 885 $cm^{-1}$ was observed with the 632.8 and 514.5 nm excitation, so there is probably weak absorption in the range 550–650 nm as seen in the Mo(VI) spectra of **4a** and **5** (<650 nm). A stronger intensity is thus expected when excited with 550 nm irradiation. In the case of antisymmetric $W^{VI}{=}O$ stretching at 843 $cm^{-1}$, the intensity was only slightly changed between 632.8 and 457.9 nm ($I/I_{483\ cm^{-1}}$ = 2.3–1.8). Thus, solely the totally symmetric mode can experience Raman intensity enhancement in this case. For the $\nu(W^{VI}{-}S)$ band at 354 $cm^{-1}$, the resonance maximized with 476.5 nm excitation ($I/I_{483\ cm^{-1}}$ = 10.1) and slightly enhanced at with 632.8 nm excitation ($I/I_{483\ cm^{-1}}$ = 1.8).

**$(NEt_4)_2[Mo^{VI}O_2(S_2C_6H_4)_2]$ (4a).** In the absorption spectrum, the maxima were observed at 335 nm ($\epsilon$ = 9500 $M^{-1}$ $cm^{-1}$), 430 nm (sh, $\epsilon$ = 2900 $M^{-1}$ $cm^{-1}$), and 533 nm ($\epsilon$ = 1500 $M^{-1}$ $cm^{-1}$). In the excitation profile of the $\nu_s(Mo^{VI}{=}O)$ band at 858 $cm^{-1}$, the maximum was observed near 632.8 nm ($I/I_{483\ cm^{-1}}$ = 11.6). The dispersion shape maximum also appears at 476.5 nm. For the $\nu_{as}(Mo^{VI}{=}O)$ band at 829 $cm^{-1}$, the maxima are at 632.8 nm ($I/I_{483\ cm^{-1}}$ > 1.9) and 488.0–476.5 nm ($I/I_{483\ cm^{-1}}$ = 1.8). For the $\nu(Mo^{VI}{-}S)$ band at 356 $cm^{-1}$, an intensity maximum was observed between 514.5 and 632.8 nm ($I/I_{483\ cm^{-1}}$ > 1.9), and a small maximum was observed at 488.0 nm ($I/I_{483\ cm^{-1}}$ = 1.6), which is the same wavelength as that for the $\nu_s(Mo^{VI}{=}O)$ band.

**$(NEt_4)_2[Mo^{VI}O_2(S_2C_6H_3Me)_2]$ (5).** In the electronic spectrum, the absorption maxima were observed at 333 nm ($\epsilon$ = 7000 $M^{-1}$ $cm^{-1}$), 420 nm (sh, $\epsilon$ = 2400 $M^{-1}$ $cm^{-1}$), and 533 nm ($\epsilon$ = 1400 $M^{-1}$ $cm^{-1}$). The enhancement maximum of a $\nu_s(Mo^{VI}{=}O)$ band at 863 $cm^{-1}$ was expected to be near 632.8 nm ($I/I_{483\ cm^{-1}}$ = 9.4). For the $\nu_s(Mo^{VI}{=}O)$ band at 496.5 nm, the small maximum was observed ($I/I_{483\ cm^{-1}}$ = 9.7), and the strongest enhancement was expected to be at a shorter wavelength than 457.9 nm ($I/I_{483\ cm^{-1}}$ > 12.3). For the $\nu_{as}(Mo^{VI}{=}O)$ band at 835 $cm^{-1}$, a weaker enhancement was observed than that of $\nu_s(Mo^{VI}{=}O)$. Also maxima were expected to be observed near 632.8 nm ($I/I_{483\ cm^{-1}}$ = 3.3) and at a shorter wavelength than 457.9 nm ($I/I_{483\ cm^{-1}}$ > 6.4). The intensity of $\nu(Mo^{VI}$-S) band at 358 $cm^{-1}$ was maximized by irradiation at 496.5 nm ($I/I_{483\ cm^{-1}}$ = 1.6) and a similar intense band was observed at shorter wavelength than 457.9 nm ($I/I_{483\ cm^{-1}}$ > 1.5).

In conclusion, the excitation profiles of the $\nu_s(M^{VI}{=}O)$ band show clear enhancements near 600 nm (700–500 nm) in the lowest-energy region of LMCT absorption bands in all $(M^{VI}O_2)^{2+}$ dithiolate complexes, **1**, **3a**, **4a**, and **5**. In the same region, relatively weak enhancements were obtained for the $\nu(M^{VI}{-}S)$ band.

**Raman Spectra of $(M^{IV}O)^{2+}$ (M = W and Mo) Complexes 6, 8, and 9.** Figure 6a–c shows Raman bands of $\nu(M^{IV}{=}O)$, $\nu(M^{IV}{-}S)$, and $\nu(C{=}C)$ for **6**, **8**, and **9**. The $(M^{IV}{=}O)^{2+}$ complexes exhibit Raman bands at 948, 903, and 905 $cm^{-1}$, respectively. These bands are assignable to the vibrations related to $M^{IV}{=}O$ bands.[22,35,42] Furthermore, Raman bands are also observed at 344, 370, 356 $cm^{-1}$ for **6**, **8**, and **9**, respectively. These bands are associated with the vibrations of $M^{IV}{-}S$ bands.[22,32,35,42]

The $Mo^{IV}{=}O$ frequency for **6**, 948 $cm^{-1}$, is very high compared to that of the other $(Mo^{IV}O)^{2+}$ dithiolate complexes **7** and **9** (910 and 904 $cm^{-1}$, respectively), whereas the lower $M^{IV}{-}S$ frequency was observed for **6** at 344 $cm^{-1}$ than for **7** and **9** (344 and 393 $cm^{-1}$, respectively). These are the results of competition for vacant $d\pi$-orbitals on the metal ion where weak $Mo^{IV}{-}S$ $\pi$-bonding strengthens $Mo^{IV}{=}O$ $\pi$-bonding.[22] The weak $Mo^{IV}{-}S$ $\pi$-bonding for **6** is attributable to the strong electron withdrawing, CN groups.

The $\pi$-donor competing feature was also observed when compared with W(IV) and Mo(IV) complexes **8** and **9**, respectively. The $\nu(W^{IV}{=}O)$ and the $\nu(W^{IV}{-}S)$ band for **8** are

(42) Ellis, S. R.; Collison, D.; Garner, C. D. *J. Chem. Soc., Chem. Commun.* **1986**, 1483.

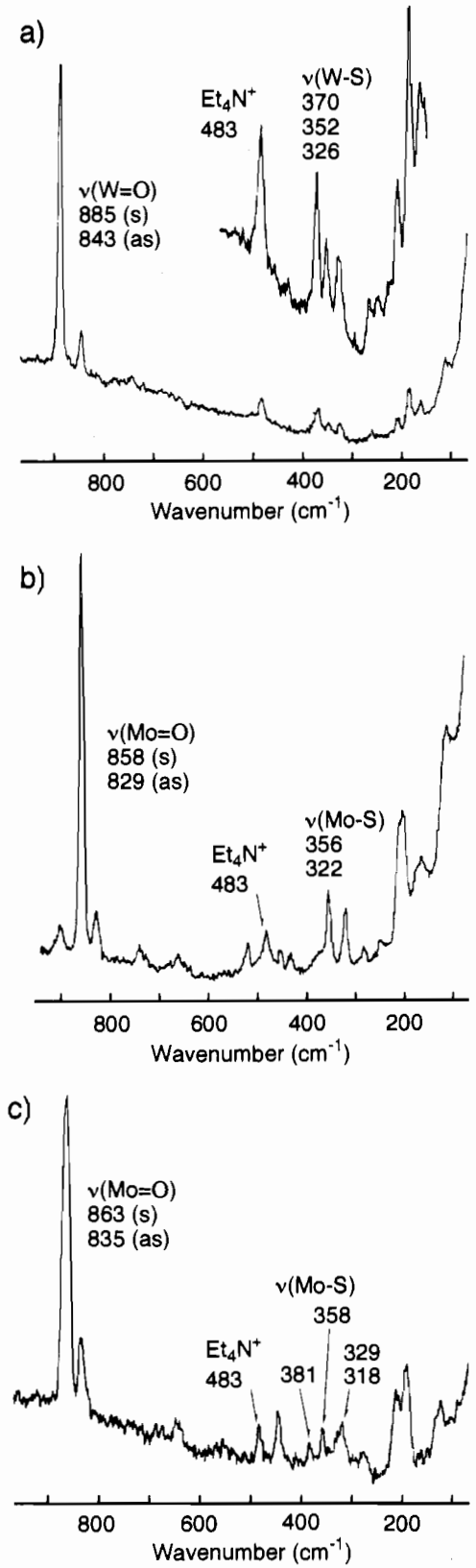


**Figure 3.** Raman spectra of $(M^{VI}O_2)^{2+}$ (M = Mo and W) thiolate complexes in the solid state, KBr disk. (a) $(NEt_4)_2[W^{VI}O_2(S_2C_6H_4)_2]$ (**3a**) (514.5 nm excitation, 100 mW laser power, 5 $cm^{-1}$ slit width, 10 s dwell time/5.0 $cm^{-1}$ step (2 s dwell time/1.0 $cm^{-1}$ step for vertical-scale-expanded spectra), 16 scans). (b) $(NEt_4)_2[Mo^{VI}O_2(S_2C_6H_4)_2]$ (**4a**) (514.5 nm excitation, 100 mW, laser power, 5 $cm^{-1}$ slit width, 1 s dwell time/5.0 $cm^{-1}$ step, 32 scans). (c) $(NEt_4)_2[Mo^{VI}O_2(S_2C_6H_3Me)_2]$ (**5**) (514.5 nm excitation, 100 mW laser power, 5 $cm^{-1}$ slit width, 1 s dwell time/5.0 $cm^{-1}$ step, 54 scans).

905 and 370 $cm^{-1}$, respectively, whereas the $\nu(Mo^{IV}{=}O)$ and the $\nu(Mo^{IV}{-}S)$ band for **9** are 904 and 356 $cm^{-1}$, respectively.

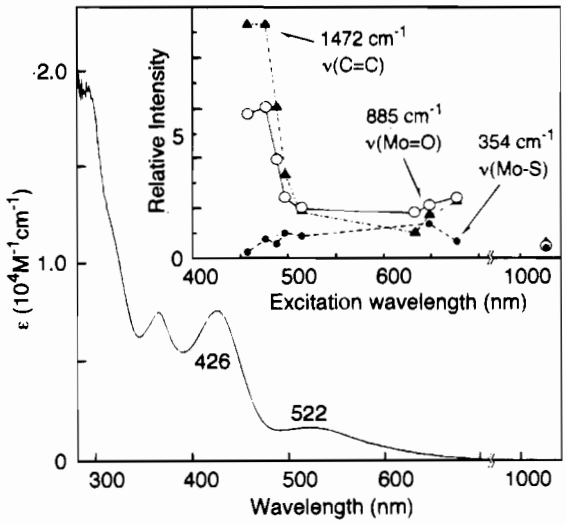


**Figure 4.** Raman excitation profiles and absorption spectra of $(PPh_4)_2[Mo^{VI}O_2(S_2C_2(CN)_2)_2]\cdot 2MeOH$ (**1**). Relative intensity refers to the enhancement normalized to the band associated with countercation $Ph_4P^+$ (1005 $cm^{-1}$).

**Table 2.** Wavenumbers ($cm^{-1}$) of the Raman Bands of $(M^{IV}O)^{2+}$ (M = Mo and W) Thiolate Complexes, **6**, **7**, **8**, and **9**

| complex | $\nu_s$-(M=O) | ν-(M–S) | ν-(C=C) |
|---|---|---|---|
| $(PPh_4)_2[Mo^{IV}O(S_2C_2(CN)_2)_2]$ (**6**) | 948 | 344 | 1491 |
| $(NEt_4)_2[Mo^{IV}O(S_2C_2(COOMe)_2)_2]$ (**7**) (in $CH_2Cl_2$, Subramanian et al.,[22] 1990) | 910 | 393 | 1535 |
| $(NEt_4)_2[W^{IV}O(S_2C_6H_4)_2]$ (**8**) | 905 | 370 | |
| $(NEt_4)_2[Mo^{IV}O(S_2C_6H_4)_2]$ (**9**) | 904 | 356 | |

**Table 3.** Comparison of Rate Constants in the Oxidation[a] of $(Mo^{IV}O)^{2+}$ Dithiolates **6** and **9** with $Me_3NO$[42]

| complex | $k_{obs}$ ($s^{-1}$) |
|---|---|
| $(PPh_4)_2[Mo^{IV}O(S_2C_2(CN)_2)_2]$ (**6**) | 1.16 (±0.05) × $10^{-4}$ |
| $(NEt_4)_2[Mo^{IV}O(S_2C_6H_4)_2]$ (**9**) | 5.7 (±0.4) × $10^{-3}$ |

[a] Reaction conditions: [Mo] = 1 mM, $[Me_3NO]$ = 10 mM, in DMF at 27 °C. Data were analyzed by pseudo-first-order kinetics, $d[Mo^{IV}]/dt = -k_{obs}[Mo^{IV}]$.

Ellis et al.[42] have already reported the Raman bands of **9**. The trend in $\nu(M^{IV}{-}S)$ wavenumber difference ($\Delta$(**8**–**9**) = +14 $cm^{-1}$) is consistent with the $M^{IV}{-}S$ bond length ($\Delta$(**8**–**9**) = −0.016 Å) in both crystal structures.[17,42] The observed higher-frequency band and the short bond length of $W^{IV}{-}S$ suggest the presence of a stronger $\pi$-interaction between W(IV) and the thiolate ligand.

**Preparative Study of $(Mo^{VI}O_2)^{2+}$ Dithiolene Complexes 1 and 2.** In the previous study, we synthesized $(PPh_4)_2[Mo^{VI}O_2(S_2C_2(CN)_2)_2]\cdot 2MeOH$ (**1**) by the O-atom transfer from trimethylamine *N*-oxide ($Me_3NO$) to $(PPh_4)_2[Mo^{IV}O(S_2C_2(CN)_2)_2]$ (**2**). The structures of both **1** and **2** have been determined by X-ray crystallography.[16,18] The obtained Raman bands of $\nu(Mo^{VI}{=}O)$, $\nu(Mo^{VI}{-}S)$, and $\nu(C{=}C)$ for **1** and **2** are shown in Table 4.

Figures 7a and 7b show the spectroscopic time course of reaction of the Mo(IV) complexes **6** and **7**, respectively, with $Me_3NO$ at the ratio $[Mo(IV)]_0/[Me_3NO]_0$ = 1/10 (mol/mol) in DMF. As expected for the spectra of the Mo(IV) complex **6**, the maximum at 368 nm diminishes with time, showing tight isosbestic points at 358 and 375 nm. After 6 h, the final spectrum, with three bands at $\lambda_{max}$ = 366, 420, and 522 nm, demonstrates a nearly quantitative formation (98%) of the $[Mo^{VI}O_2(S_2C_2(CN)_2)_2]^{2-}$ anion (**1**). From the analysis of the time conversion curve obtained by monitoring the 420 nm absorption maximum, by pseudo-first-order kinetics, a rate

**Table 4.** Comparison of the Raman Bands ($cm^{-1}$) of Dithiolene Complexes **1**, **2**, **6**, and **7**

| complex | $\nu$-(Mo=O) | $\nu$-(Mo−S) | $\nu$-(C=C) |
|---|---|---|---|
| $(PPh_4)_2[Mo^{VI}O_2(S_2C_2(CN)_2)_2]\cdot 2MeOH$ (**1**) | 885 | 354 | 1472 |
| | 851 | 330 | |
| | | 313 | |
| $(PPh_4)_2[Mo^{IV}O(S_2C_2(CN)_2)_2]$ (**6**) | 948 | 344 | 1491 |
| $(NEt_4)_2[Mo^{VI}O_2(S_2C_2(COOMe)_2)_2]$ (**2**) | 870 | | 1503 |
| (in DMSO, *in situ* formation) | 838 | | |
| $(NEt_4)2[Mo^{IV}O(S_2C_2(COOMe)_2)_2]$ (**7**) | 910 | 393 | 1535 |
| (in $CH_2Cl_2$, Subramanian et al.,[22] 1990) | | | |
| DMSO reductase (oxidized state) | | | 1575 |
| (reduced state) | | | 1568 |
| (Gruber et al.,[13] 1990) | | | |
| $[Mo^{VI}(S_2C_2(CF_3)_2)_3]$ | | | 1455 |
| $(PPh_4)_2[Mo^{IV}(S_2C_2(CF_3)_2)_3]$ | | | 1538 |
| (solid-state IR spectra, Davison et al.,[54] 1964) | | | |

constant, $k_{obs} = 1.15\ (\pm\ 0.05) \times 10^{-4}\ s^{-1}$ [43] was obtained in the initial stage (Table 3). Thus, we concluded that the reaction proceeds by a simple bimolecular mechanism[35,44] as shown below.

$$[Mo^{IV}O(S_2C_2(CN)_2)_2]^{2-} + Me_3NO \rightarrow$$
(anion part of **6**)

$$[Mo^{VI}O_2(S_2C_2(CN)_2)_2]^{2-} + Me_3N$$
(anion part of **2**)

On the other hand, in the reaction of the $(Mo^{IV}O)^{2+}$ complex **7**, the $(Mo^{VI}O_2)^{2+}$ complex $(NEt_4)_2[Mo^{VI}O_2(S_2C_2(COOMe)_2)_2]$ (**2**) could not be stably formed, but the $(Mo^{VI}O_2)^{2+}$ species was detected only transiently by absorption spectroscopy. As shown in Figure 7b, the absorption maxima of **7** increase initially in intensity at about 300−600 nm, showing an isosbestic point at 285 nm. In 10 h after the addition of $Me_3NO$, the spectrum with four $\lambda_{max}$ (390, 358, 417 and 530 nm) exhibit a typical features for the dioxomolybdenum(VI) thiolate complex which resemble those of **4a**.[16,18] After the appearance of the $(Mo^{VI}O_2)^{2+}$ thiolate absorptions, each peak at 390, 358, 417, and 530 nm decreases gradually. Finally, 24 h after the addition of $Me_3NO$, the reaction mixture gives only one maximum, at 337 nm. Those spectral changes indicate that further oxidation at the thiolate ligand of the Mo(VI) complex **2** occurs. This behavior is quite different from the observed stability for the Mo(VI) complex **1**. Thus, the reaction process is proposed to be as follows.

$$[Mo^{IV}O(S_2C_2(COOMe)_2)_2]^{2-} + Me_3NO \rightarrow$$
(anion of **7**)

$$[Mo^{VI}O_2(S_2C_2(COOMe)_2)_2]^{2-} + Me_3N \xrightarrow[Me_3NO]{}$$
(anion part of **2**)

unidentified thiolate−oxidzed product

To characterize the intermediate product, the Raman spectra of the reaction mixture in DMSO at 27 °C were measured. The Raman spectra, which were recorded during a period of 10.5−12.0 h after the mixing, are shown in Figure 8. The typical *cis*-dioxomolybdenum(VI) structure was detected, as indiciated by the two bands at 870 and 838 $cm^{-1}$ which are assignable to $\nu_s(Mo^{VI}{=}O)$ and $\nu_{as}(Mo^{VI}{=}O)$, respectively. A band associated with dithiolene $\nu$(C=C) stretching was observed at 1503 $cm^{-1}$. In the spectra, the $\nu(Mo^{IV}{=}O)$ and $\nu$(C=C) bands at 910 and 1535 $cm^{-1}$, respectively, which were observed for the Mo(IV) complex **7**, were not detected, although those bands are reported to be somewhat weaker Raman scatterers.[22] At the same time, a $^1H$ NMR spectrum was measured in DMSO-$d_6$. The Mo(VI) complex **2** was detected up to 70% in this system. The yield was calculated from the newly appearing $CH_3$ signal at 3.57 ppm (singlet), which is attributable to the Mo(VI) complex **2**. Thus, we concluded that the intermediate absorption maxima ($\lambda_{max}$) at 390, 358, 417, and 537 nm in DMF come from the $(Mo^{VI}O_2)^{2+}$ dithiolate complex $(NEt_4)_2[Mo^{VI}O_2(S_2C_2(COOMe)_2)_2]$ (**2**).

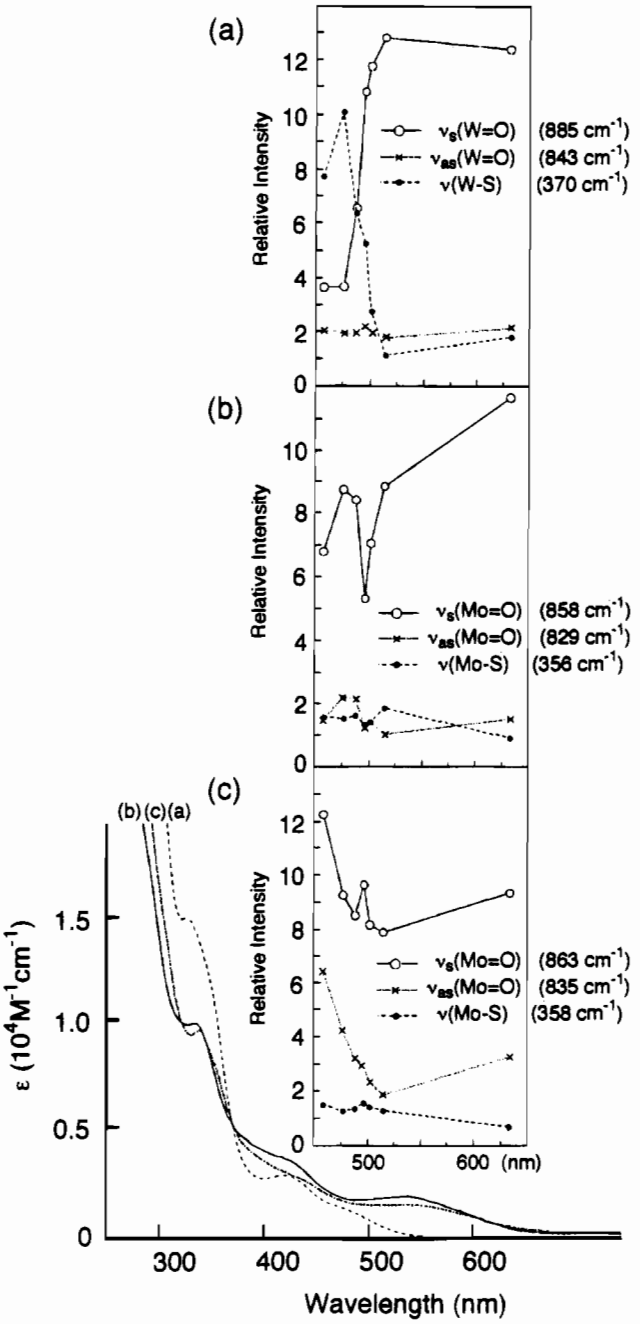


**Figure 5.** Raman excitation profiles and absorption spectra for bis(benzenedithiolato) complexes of dioxotungsten(VI) and dioxomolybdenum(VI). (a) $(NEt_4)_2[W^{VI}O_2(S_2C_6H_4)_2]$ (**3a**). (b) $(NEt_4)_2[Mo^{VI}O_2(S_2C_6H_4)_2]$ (**4a**). (c) $(NEt_4)_2[Mo^{VI}O_2(S_2C_6H_3Me)_2]$ (**5**). Absorption spectra are recorded in DMF solutions. The intensities are normalized relative to the band associated with $Et_4N^+$ (483 $cm^{-1}$).

## Discussion

**Raman Spectra and Raman Excitation Profiles for $(M^{VI}O_2)^{2+}$ (M = Mo and W) Complexes 1, 3a, 4a, and 5.**

(43) All errors in parentheses are random errors estimated at the 99% confidence level (2.5$\sigma$).
(44) Schultz, B. E.; Holm, R. H. *Inorg. Chem.* **1993**, *32*, 4244.

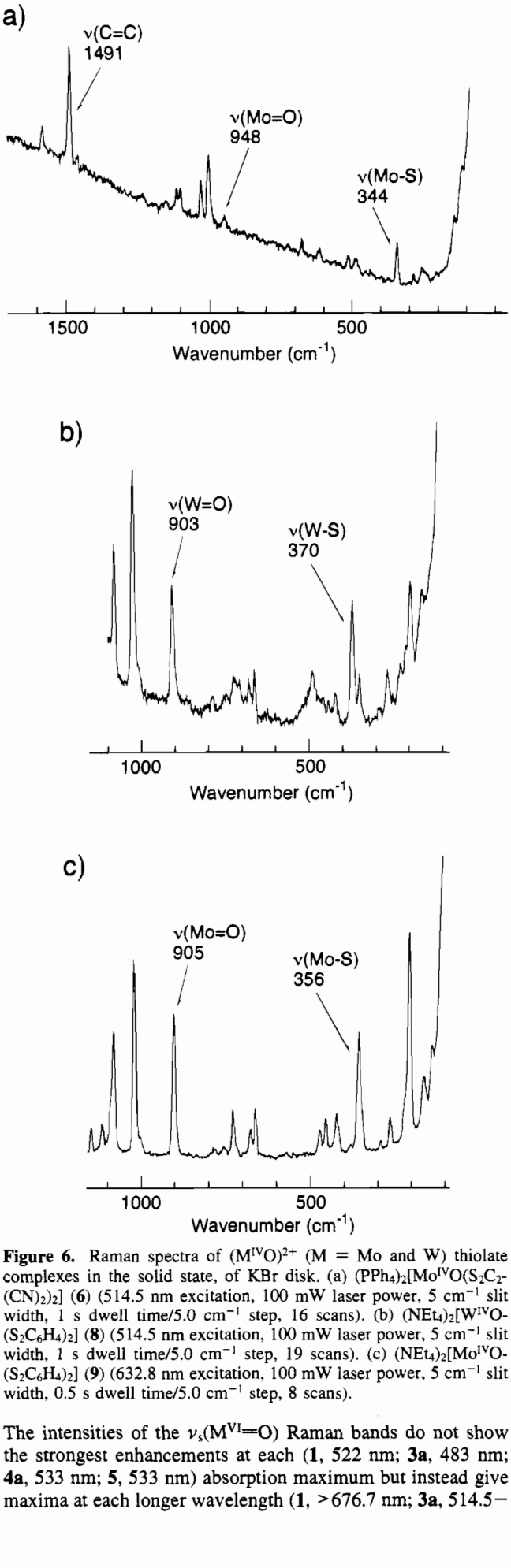


**Figure 6.** Raman spectra of $(M^{IV}O)^{2+}$ (M = Mo and W) thiolate complexes in the solid state, of KBr disk. (a) $(PPh_4)_2[Mo^{IV}O(S_2C_2(CN)_2)_2]$ (**6**) (514.5 nm excitation, 100 mW laser power, 5 $cm^{-1}$ slit width, 1 s dwell time/5.0 $cm^{-1}$ step, 16 scans). (b) $(NEt_4)_2[W^{IV}O(S_2C_6H_4)_2]$ (**8**) (514.5 nm excitation, 100 mW laser power, 5 $cm^{-1}$ slit width, 1 s dwell time/5.0 $cm^{-1}$ step, 19 scans). (c) $(NEt_4)_2[Mo^{IV}O(S_2C_6H_4)_2]$ (**9**) (632.8 nm excitation, 100 mW laser power, 5 $cm^{-1}$ slit width, 0.5 s dwell time/5.0 $cm^{-1}$ step, 8 scans).

The intensities of the $\nu_s(M^{VI}{=}O)$ Raman bands do not show the strongest enhancements at each (**1**, 522 nm; **3a**, 483 nm; **4a**, 533 nm; **5**, 533 nm) absorption maximum but instead give maxima at each longer wavelength (**1**, >676.7 nm; **3a**, 514.5–632.8 nm; **4a**, near 632.8 nm; **5**, near 632.8 nm), as shown in Figures 4 and 5. The $\nu(M^{VI}{-}S)$ bands show weaker enhancements than the $\nu_s(M^{VI}{=}O)$ bands in the same wavelength region (**1**, 647.9 nm; **3a**, near 632.8 nm; **4a**, 514.5 nm; **5**, 496.5 nm).

The lowest-energy absorption maxima at 480–530 nm for **1**, **3a**, **4a**, and **5** are due to the charge-transfer (CT) transition bands because those complexes have $d^0$ configuration. The lowest energy transition can be assigned, therefore, as the HOMO → LUMO transition. To clarify the LMCT transition, orbital diagrams were constructed by the *ab initio* Hartree–Fock calculation with the STO-3G basis set. Figure 9 shows the orbital diagrams (HOMO and LUMO) for the anion structure of **4b**. The HOMO wave function character is found to be an orbital based on the thiolate ligands (mainly *trans* to oxo). The LUMO character is made up of the metal d-based orbital. In the LUMO, the Mo d-orbital is antibonding with the O p$\pi$-orbital of the oxo ligand. For the other ligand or metal complexes **1** (1,2-dicyanoethylene-1,2-dithiolate) and **3b** (W(VI)), similar orbital descriptions are obtained by *ab initio* Hartree–Fock and extended Hückel calculations, respectively. Therefore, the lowest-energy band in the UV/vis spectra is ascribable to the electronic transition from the thiolate p$\pi$-orbital to the metal d-orbital.

One question comes up here. Why does the $\nu_s(M^{VI}{=}O)$ band show enhanced intensity at that lowest-energy band (S → M(VI) CT band)? The answer to be this question is given by considering of the excited electronic state. According to the report by Hirakawa et al.,[45,46] the intensity enhancement during the resonance Raman process is observed from those modes in which the variations of nuclei positions correspond to the distortions experienced by the molecule when going to its resonant excited state. For example, in the case of $\beta$-carotene,[47] the $\pi \rightarrow \pi^*$ transition leads to a large intensity gain for those modes at 1523 and 1156 $cm^{-1}$ involving stretching of the C=C and C–C bonds, respectively, because these bond distances change (elongation and shrinkage, respectively) appreciably in the $\pi^*$ state. However, the C–H bonds are little perturbed on going from the $\pi$ to the $\pi^*$ state; consequently, C–H stretching modes show minimal intensity variation as the resonance condition is approached. The theoretical background for this intensity enhancement due to vibronic coupling has been described.[45] This type of Raman line enhancement was also reported for $NH_3$,[46] methylamine,[46] formamide ($\pi \rightarrow \pi^*$ transition),[46] *cis*-dichloroethylene ($\pi \rightarrow \pi^*$ transition),[46] propargyl alcohol ($\pi \rightarrow \pi^*$ transition),[46] $\beta$-adenosine-5'-phosphoric acid ($\pi \rightarrow \pi^*$ transition),[48] and $K_2CrO_4$ (LMCT transition).[49] In our case, at the lowest-excited electronic state by the lowest-energy LMCT transition, one of the electrons of the HOMO which is the thiolate-based orbital, is excited to the LUMO (antibonding to the M=O), and therefore the M=O bond is expected to be longer. Similar M=O bond elongation is also anticipated for the symmetric M=O stretching vibration ($\nu_s(M^{VI}{=}O)$) in the *cis*-$(M^{VI}O_2)^{2+}$ structure. The observed intensity enhancements for the $\nu_s(M^{VI}{=}O)$ Raman bands are, therefore, attributable to the coupling of the same geometrical change in both the normal mode vibration of $\nu_s(M^{VI}{=}O)$ and the M=O bond elongation during electronic excitation, when

(45) Tsuboi, M.; Hirakawa, A. Y. *J. Raman Spectrosc.* **1975**, *5*, 75.
(46) Hirakawa, A. Y.; Tsuboi, M. *Science.* **1975**, *188*, 359.
(47) (a) Tasumi, M; Inagaki, F; Miyazawa, T. J. Chem. Phys. **1971**, *55*, 4438. (b) Inagaki, F.; Tasumi, M.; Miyazawa, T. *J. Mol. Spectrosc.* **1974**, *50*, 286. (c) Carey, P. R. *Biochemical Applications of Raman and Resonance Raman Spectroscopies*; Academic Press: New York, 1982, pp. 45; 47.
(48) Tsuboi, M.; Hirakawa, A. Y.; Nishimura, Y. *J. Raman Spectrosc.* **1974**, *2*, 609.
(49) Tsuboi, M.; Hirakawa, A. Y. *J. Mol. Spectrosc.* **1975**, *56*, 146.

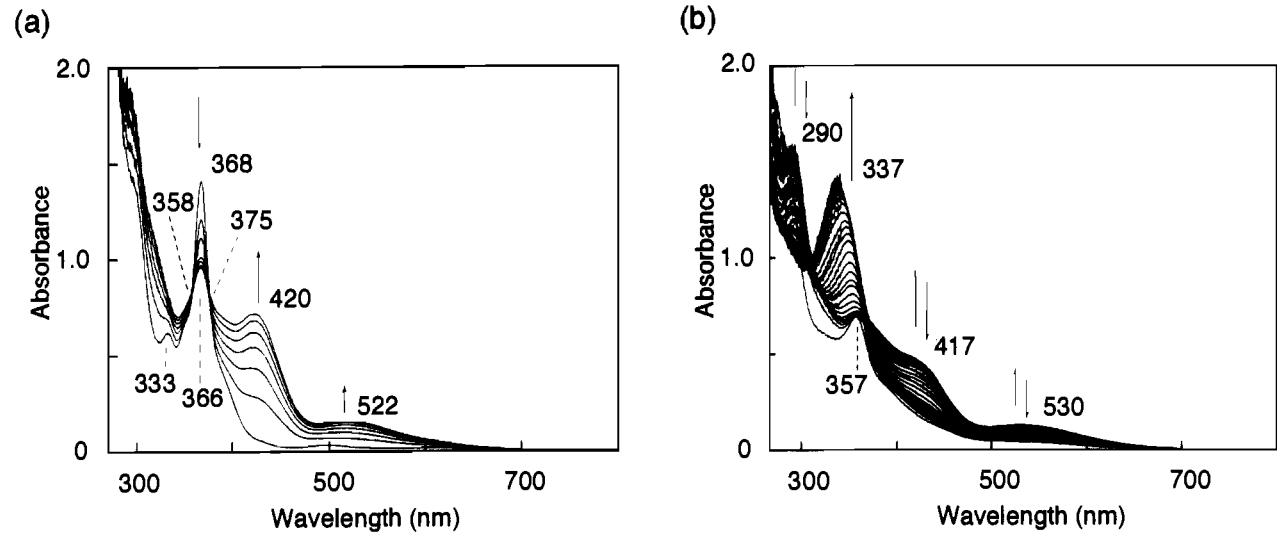


**Figure 7.** UV/vis spectral change (measured every 1 h) in the oxidation of (a) $(PPh_4)_2[Mo^{IV}O(S_2C_2(CN)_2)_2]$ (**6**) and (b) $(NEt_4)_2[Mo^{IV}O(S_2C_2(COOMe)_2)_2]$ (**7**) ([Mo] = 1 mM) with $Me_3NO$ ([$Me_3NO$] = 10 mM) in DMF at 27 °C (cell length = 1 mm).

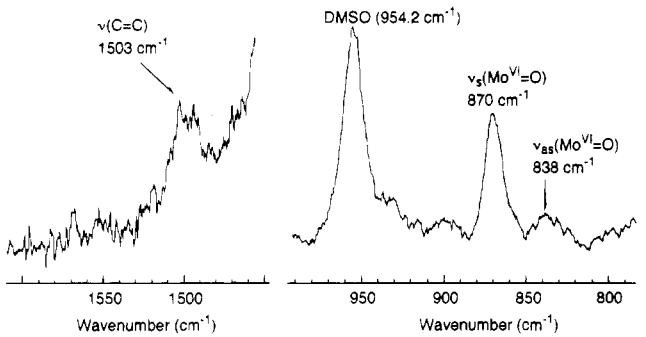


**Figure 8.** Raman spectra of $\nu$(Mo=O) and $\nu$(C=C) region for the *in situ* formed $(NEt_4)_2[Mo^{VI}O_2(S_2C_2(COOMe)_2)_2]$ (**2**) complex. Conditions: [Mo] = 4 mM in DMSO solution, 50 mW laser power, 5 $cm^{-1}$ slit width, 1 s dwell time/1.0-$cm^{-1}$ step.

the exciting frequency is brought closer to the frequency of the lowest-energy LMCT band.

The labilization of the Mo=O bond at the lowest-energy LMCT transition is also expected by consideration of electrochemical behavior. Dioxomolybdenum(VI)[50] and dioxotungsten(VI) complexes having thiolate ligands *trans* to the $M^{VI}$=O groups exhibit an irreversible reduction peak due to the O-atom release after reduction to the M(V) species. For **3a**, **4a**, and **5**, cyclic voltammograms in DMF solutions exhibit irreversible reduction peaks at −1.26, −1.03 and −1.15 V (concomitant with a −0.99 V irreversible peak) (vs SCE), respectively, presumably assignable to the Mo(VI)/Mo(V) redox process and the successive O-atom releasing reactions when scanned in the cathodic direction. On the contrary, the thioether complex $[Mo^{VI}O_2(dttd)]$ (**10**), which has two thioether ligands located at the *trans* position of the $Mo^{VI}$=O bonds, exhibits a reversible Mo(VI)/Mo(V) redox couple at −0.82 V (vs SCE)[37] without the release of one of the oxo ligands. The different electrochemical behavior is possibly due to the strengthening of the $Mo^{VI}$=O bond by weakening of the $Mo^{VI}$-S bond *trans* to $Mo^{VI}$=O with the less electron-donating thioether ligand in **10**, as observed in the higher frequencies of the $\nu(Mo^{VI}=O)$ bands. Theoretical analysis also explains the electrochemical behavior. The calculated bond orders (Mülliken bond order) for the $Mo^{VI}$=O bond are 2.13809 in the thiolato complex, the anion part of **4b**, and 2.37978 in the thioether complex **10** (Table 5).

(50) De Hayes, L. J.; Faulkner, H. C.; Doub, W. H., Jr.; Sawyer, D. T. *Inorg. Chem.* **1975**, *14*, 2110.

**Table 5.** Calculated Mo=O Bond Order Change in One-Electron Reduction[a]

| | Mo=O bond order (mean) |
|---|---|
| $[Mo^{VI}O_2(S_2C_6H_4)_2]^{2-}$ (anion part of **4b**) | 2.13089 |
| $[Mo^{V}O_2(S_2C_6H_4)_2]^{3-}$ (anion part of **4b**+ e-) | 2.10129 |
| $[Mo^{VI}O_2(dttd)]$ (**10**) | 2.37978 |
| $[Mo^{V}O_2(dttd)]^-$ (**10** + $e^-$) | 2.20518 |

[a] Hartree−Fock calculation with STO-3G basis set was used.

When one electron is added to each model structure (half-occupation of LUMO), the bond orders are decreased to 2.10129 in the anion part of **4b** and to 2.20518 in **10**. The thioether complex **10** shows still larger Mo=O bond order on the one-electron reduction than in the case of **4b**. This agrees well with the electrochemical behavior, which shows Mo=O bond activation on one-electron reduction of the thiolato complex **4a** and no activation in the case of the thioether complex **10**. In the case of **10**, the enhancement profile for the $\nu_s(Mo^{VI}=O)$ band was not fully plotted (400−500 nm) for all of its absorption spectrum,[22] and therefore further research in the region of 500−650 nm seems to be required. From a theoretical calculation, the LUMO is antibonding at the $M^{VI}$=O part. The enhancement of the $\nu_s(Mo^{VI}=O)$ band is anticipated at the lowest-energy region of the LMCT band (near 500 nm) of **10**. Indeed, the tail of the enhancement was seen around 500 nm. Probably, the absolute intensity for **10** is lower than that of the thiolato complex **3** because the oxo ligand is not activated by the thiolato coordination.

The resonance Raman study of active-site models revealed that the reactive oxo ligand shows the strong enhancement of Raman bands, because the reactive $M^{VI}$=O bond can deform largely during the lowest-energy LMCT transition. Therefore, the bond deformation (elongation and shrinkage) couples strongly with similar geometrical change in the symmetric stretching of the M=O bond during the resonance Raman process. Not only these M=O bands but also the bands associated with the activated or reactive bond are expected to be enhanced in resonance Raman spectra. Moreover, the electronic structures of those important bonds will appear as a bond deformation or a conformational change during the charge-transfer transition with the use of resonance Raman spectroscopy in various oxo-transfer enzymes and electron-transfer proteins. The study of oxo-transfer enzymes is one suitable example. Mo

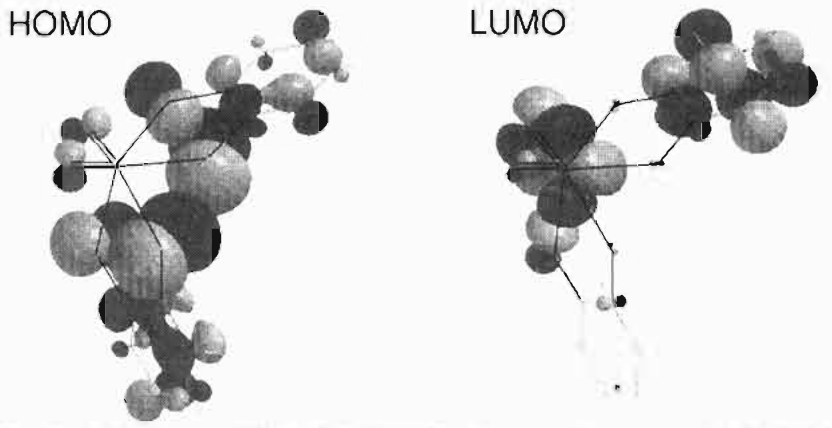


**Figure 9.** HOMO and LUMO orbital diagrams for $[Mo^{VI}O_2(S_2C_2(CN)_2)_2]^{2-}$ (Hartree-Fock calculation with STO-3G basis set).

and W oxidoreductases have reactive $M^{VI}$=O bonds which are probably activated strongly by the mutual *trans* influence with thiolate.[15-19] Cytochrome P-450 has the reactive $Fe^{IV}$=O and O—O[51] bonds during the catalytic cycle which are also labilized by the mutual *trans* influence of cysteine thiolate. Those activated bonds will show bond elongation and a highly enhanced Raman line when irradiated in the lowest-energy region of charge-transfer bands. Another applicable example is the study of electron-transfer proteins. Iron−sulfur proteins (rubredoxin,[52] etc.), blue copper proteins (plastocyanin,[53] etc.) and flavo proteins (flavodoxin etc.) have weak interactions such as NH···S hydrogen bonds, aromatic···thiolate interactions, metal-sulfur $\pi$- and $\sigma$-bonding, and aromatic···aromatic interactions. A combination of specially designed structures has been thought to provide an electron-transfer pathway. The structural changes during the charge-transfer transition will appear in the Raman excitation profiles of the various proteins.

The model complexes of electron-transfer proteins and oxo-transfer enzymes will show the characteristic bonding nature by research on the resonance Raman process. In our case, with the consideration of orbital diagrams, the Raman intensity enhancement for the $\nu_s(M^{VI}=O)$ bands elucidates activation of the $M^{VI}$=O bonds by the mutual *trans* influence which can contribute to the increase of reactivity[16-18] toward the oxo transfer.

**Raman Study for the Dithiolene Complexes 1, 2, 6, and 7.** Table 4 lists the Raman bands of $\nu$(Mo=O), (Mo—S) and $\nu$(C=C) for $(Mo^{VI}O_2)^{2+}$ and $(Mo^{IV}O)^{2+}$ dithiolato complexes **1**, **2**, **6**, and **7**. In a comparison between $(Mo^{IV}O)^{2+}$ dithiolato complexes **6** and **7**, the stronger electron-withdrawing effect of the cyano group in **6** is consistent with the trends of the Raman band wavenumber differences in $\nu(Mo^{IV}=O)$ ($\Delta$(**6**−**7**) = 38 $cm^{-1}$), $\nu(Mo^{IV}-S)$ ($\Delta$(**6**−**7**) = −49 $cm^{-1}$), and $\nu$(C=C) ($\Delta$(**6**−**7**) = −44 $cm^{-1}$), where the $Mo^{IV}$—S and C=C bonds are weakened and the $Mo^{IV}$=O bond is strengthened by the cyano group. The same trends were also observed for the $(Mo^{VI}O_2)^{2+}$ dithiolato complexes **1** and **2**, in which the C=C bond is weakened ($\Delta$(**1**−**2**) = −31 $cm^{-1}$) and the $Mo^{VI}$=O bond is strengthened ($\Delta$(**1**−**2**) = 15 $cm^{-1}$ for symmetric stretching and 13 $cm^{-1}$ for antisymmetric stretching). The weaker electron-withdrawing group, methoxycarbonyl (COOMe), on the dithiolene ligand of **2** is unable to assist the stabilization of the $Mo^{VI}$=O bonds through the $Mo^{VI}$—S—C bond. Thus, the transiently formed complex of **2** undergoes further oxidation on the thiolate ligand of the Mo(VI) complex **2** by $Me_3NO$.

One of the interesting points in the present study is the shift of Raman $\nu$(C=C) frequencies at the oxidation state. For the C=C stretching region, the resonance Raman bands in the active center of DMSO reductase have been reported at 1575 $cm^{-1}$ in the oxidized state and at 1568 $cm^{-1}$ in the reduced state. If the oxidized state has Mo(VI) and the reduced state has Mo(IV), the direction of the redox-associated frequency shift (7 $cm^{-1}$, when the active site is oxidized) is not in agreement with the shift observed for the model complexes as listed in Table 4. The C=C band frequency is observed to decrease by 19 $cm^{-1}$ for **6** and **1** and by 32 $cm^{-1}$ for **7** and **2** when the model complexes are oxidized from Mo(IV) to Mo(VI). In the case of the tris(dithiolate) complexes, the C=C band frequency decreases (83 $cm^{-1}$) by oxidation at the Mo atom; i.e., $[Mo^{IV}(S_2C_2(CF_3)_2)_3]^{2-}$ to $[Mo^{VI}(S_2C_2(CF_3)_2)_3]$ (Table 4).[54] Thus, the C=C bond order should be increased by back-donation from the metal d$\pi$−orbital through the $M^{IV}$—S—C bond. The bond order increase is not in agreement with the estimation by Gruber et al.[13] Therefore, the observed trend of the $\nu$(C=C) mode in DMSO reductase is very anomalous when compared with that of the model complexes.

There are four possible explanations for the cause of the diverse shifts in $\nu$(C=C) band frequencies—(1) electronic coupling of the redox-active pterin dithiolene ligand and the molybdenum ion, (2) vibrational coupling with the pterin mode, (3) the vibrational coupling with the S—C—C bending mode, and (4) NH···S hydrogen bonding in the dithiolate-all which could change with oxidation state. In addition, the dithiolene model complexes do not simulate exactly the enzyme active site because the dithiolene model complexes lack the redox-active pterin side chain and have electron-withdrawing groups attached to the ene-1,2−dithiolates. Any or all of these, including protein contacts, could be the cause of the differences in the C=C stretches observed between the cofactor and the models upon oxidation state change. In this report, we will discuss those four candidates for the cause of the diverse shifts in $\nu$(C=C) band frequencies.

The first candidate is the electronic coupling of the pterin dithiolene ligand and the molybdenum ion. If the protonation/deprotonation and redox reaction processes of the pterin group

(51) (a) Dawson, J. H.; Holm, R. H.; Trudell, J. R.; Barth, G.; Linder, R. E.; Bunnenberg, E.; Djerassi, C. *J. Am. Chem. Soc.* **1976**, *98*, 3707. (b) Dawson, J. H.; Sono, M. *Chem. Rev.* **1987**, *87*, 1255. (c) Dawson, J. H. *Science* **1988**, *240*, 433.

(52) (a) Sun, W. Y.; Ueyama, N; Nakamura, A. *Inorg. Chem.* **1993**, *32*, 1095. (b) Ueyama, N; Sun, W. Y.; Nakamura, A. *Inorg. Chem.* **1992**, *31*, 4053. (c) Ueyama, N.; Sugawara, S.; Tatsumi, K.; Nakamura, A. *Inorg. Chem.* **1987**, *26*, 1978.

(53) (a) Lowery, M. D.; Guckert, J. A.; Gebhard, M. S.; Solomon, E. I. *J. Am. Chem. Soc.* **1993**, *115*, 3012. (b) Gewirth, A. A.; Solomon, E. I. *J. Am. Chem. Soc.* **1988**, *110*, 3811.

(54) Davison, A; Edelstein, N; Holm, R. H.; Maki, A. H. *J. Am. Chem. Soc.* **1964**, *86*, 2779.

are accompanied by redox reaction at the molybdenum ion, the electronic state of the C=C bond should be affected anomalously compared with the case of the redox-inactive dithiolene ligand. Actually, Garner et al.[55] reported electrochemical behavior of $[CpCo^{III}(S_2C_2H(quinoxalin\text{-}2\text{-}yl))]$, which contains a redox-active pyrazine ring with a dithiolene substituent as models of the cofactor, and demonstrated how reduction at the metal center may be coupled to the protonation of the pyrazine ring. From the model study, they have suggested the possibility of redox cooperativity between the molybdenum ion and the pterin dithiolene ligand.

The second and third candidates, vibrational coupling with the pterin mode and with the S−C−C bending mode, are anticipated to have a small effect if the dithiolene structure receives electronic perturbation only from the molybdenum ion upon oxidation state change. This is deducible from the study by Schläpfer and Nakamoto,[33] who have done the normal-coordinate analysis of 1,2-dithiolene complexes of the type $[Ni(S_2C_2R_2)_2]^x$, where R is H, $C_6H_5$, $CF_3$, or CN and $x$ is 0, 1−, or 2−.

The fourth candidate, i.e., the NH···S hydrogen bond to the dithiolene ligand, can delocalize the electron density and strengthen the metal−thiolato bond.[55] If there is effective NH···S hydrogen bonding at the oxidized state active site, the C=C bond order and the $\nu$(C=C) band frequency should be increased. Therefore, the hydrogen bonding can explain the higher wavenumber shift of the $\nu$(C=C) band as observed in the oxidized state of DMSO reductase, 1575 $cm^{-1}$, compared with the reduced one, 1568 $cm^{-1}$. A possible role of the NH···S hydrogen bonding is as a trigger of the oxo-transfer reaction. When the hydrogen bond was formed at the dithiolene thiolato moiety, the *trans* influence will be lowered and then the activating effect on the oxo ligand is diminished.

The anomalous difference is also observed in the UV/vis spectrum for the oxidized state of DMSO reductase compared with those of $(Mo^{VI}O_2)^{2+}$ dithiolate complexes. The $(Mo^{VI}O_2)^{2+}$ dithiolate complex **4a**, ($\lambda_{max}$ ($\epsilon$) (nm ($M^{-1}$ $cm^{-1}$)) = 335 (sh, 7000), 430 (sh, 2400), 533 (1400)) lacks the absorption maximum near 720 nm which is observed for the oxidized state of DMSO reductase[57] ($\lambda_{max}$ ($\epsilon$) (nm ($M^{-1}cm^{-1}$)) ~340 (4900), 470 (2200), 450 (1600), 720 (1900)). A spectrum similar to that of the oxidized state of DMSO reductase was reported for the bis($\eta$-selenido)ditungsten(V) complex $(PPh_4)_2[W_2Se_2(Se_2C_2(COOMe)_2)_4]$,[58] which has a strong absorption maximum at 550 nm ($\epsilon$ = 16000 $M^{-1}$ $cm^{-1}$), although the maximum was shifted to the shorter wavelength due to the higher ligand field of the tungsten ion.[17,59] On the other hand, the molybdenum-containing fragment of sulfite oxidase has no absorption maximum at wavelengths longer than 600 nm ($\lambda_{max}$ (nm) = ~290, 353, 409 (sh), 464 (sh)).[57] The active site of this fragment is presumably the Mo(VI) thiolate structure, because the spectrum closely resembles the $(Mo^{VI}O_2)^{2+}$ dithiolate complex **4a**.

The range of wavenumbers for the C=C band reported for DMSO reductase is considerably higher than that in the dithiolene model complexes **1**, **2**, **6**, and **7**, (30−120 $cm^{-1}$ difference), possibly reflecting the stronger donating nature of the dithiolene ligand in the pterin cofactor. The strong donating ability is expected to cause enhanced oxidizing reactivity at the $(Mo^{VI}O_2)^{2+}$ site by the *trans* influence of sulfur coordination in the cofactor.

## Conclusion

Strong enhancement is observed for the $\nu_s(M^{VI}{=}O)$ (M = Mo and W) band in resonance with the lowest-energy region of the thiolate → metal CT transition, because the $(M^{VI}O_2)^{2+}$ structure can distort during excitation from the ground to the excited electronic state along the normal coordinate for the Raman line of $\nu_s(M^{VI}{=}O)$. Observation of the enhanced Raman bands associated with the lower-energy electronic transition was utilized to reveal the electronic structure of the important bonds in the active site of proteins and in the various model complexes. One application of this method is the study of electron-transfer pathways, which have been investigated extensively from the point of view of their electronic structure, and their associated bonds or interactions which are thought to provide a channel for electron transfer.[47,48] Thus, through the study of the molybdenum and tungsten oxidoreductase model complexes with Raman spectra, we found the essential feature of oxo activation to be due to the *trans* effect by thiolate ligation toward the oxo-transfer reaction.

**Acknowledgment.** We are grateful for financial support by JSPS Fellowships (Hiroyuki Oku; No. 1278, 1993−1994) for Japanese Junior Scientists, and by a Grant-in-Aid for Specially Promoted Research from the Ministry of Education, Science and Culture of Japan.

IC941137R

(55) Garner, C. D.; Armstrong, E. M.; Ashcroft, M. J.; Austerberry, M. S.; Birks, J. H.; Collison, D.; Goodwin, A. J.; Larsen, L.; Rowe, D. J.; Russel, J. R. In ref 1b, Chapter 7, p 98.

(56) Ueyama, N.; Okamura, T.; Nakamura, A. *J. Am. Chem. Soc.* **1992**, *114*, 8129.

(57) (a) Johnson, J. L.; Rajagopalan, K. V. *J. Biol. Chem* **1977**, *252*, 2017. (b) Bastian, N. R.; Kay, C. J.; Barber, M. J.; Rajagopalan, K. V. *J. Biol. Chem.* **1991**, *266*, 45−51.

(58) Ansari, M. A.; Mahler, C. H.; Ibers, J. A. *Inorg. Chem.* **1989**, *28*, 2669.

(59) With the replacement of the metal atom from molybdenum to tungsten, a blue shift (150 nm) was observed for monooxotungsten(V) and molybdenum(V) bis(1,2-benzenedithiolate) complexes.[17]